Exploiting the leaky-wave properties of transmission-line metamaterials for single-microphone direction finding

Hussein Esfahlani, Sami Karkar, and Hervé Lissek[a)]
Laboratoire de Traitement des Signaux LTS2, Ecole Polytechnique Fédérale de Lausanne, Station 11, CH-1015, Lausanne, Switzerland

Juan R. Mosig
Laboratoire d'Electromagnétisme et d'Antennes LEMA, Ecole Polytechnique Fédérale de Lausanne, Station 11, CH-1015, Lausanne, Switzerland

(Received 9 September 2015; revised 29 January 2016; accepted 13 March 2016; published online 30 June 2016)

A transmission-line acoustic metamaterial is an engineered, periodic arrangement of relatively small unit-cells, the acoustic properties of which can be manipulated to achieve anomalous physical behaviours. These exotic properties open the door to practical applications, such as an acoustic leaky-wave antenna, through the implementation of radiating channels along the metamaterial. In the transmitting mode, such a leaky-wave antenna is capable of steering sound waves in frequency-dependent directions. Used in reverse, the antenna presents a well defined direction-frequency behaviour. In this paper, an acoustic leaky-wave structure is presented in the receiving mode. It is shown that it behaves as a sound source direction-finding device using only one sensor. After a general introduction of the acoustic leaky-wave antenna concept, its radiation pattern and radiation efficiency are expressed in closed form. Then, numerical simulations and experimental assessments of the proposed transmission-line based structure, implementing only one sensor at one termination, are presented. It is shown that such a structure is capable of finding the direction of an incoming sound wave, from backward to forward, based on received sound power spectra. This introduces the concept of sound source localization without resorting to beam-steering techniques based on multiple sensors. © *2016 Acoustical Society of America*. [http://dx.doi.org/10.1121/1.4949544]

[ANN] Pages: 3259–3266

I. INTRODUCTION

The advent of metamaterials has opened new doors to physical and engineering applications. Following the first investigations and developments in electromagnetics, applications in other fields of physics were envisaged for such artificial structures such as optics, acoustics, mechanics, and thermodynamics. In acoustics, many novel concepts are now proposed that may prove to be beyond what was previously thought possible. Cloaking,[1] super lensing,[2] super absorbers,[3] metasurfaces,[4] or non-reciprocal devices[5,6] are some such examples.

The study on locally resonant sonic materials by Liu *et al*.[7] may be considered as the first work on acoustic metamaterials with subwavelength unit-cells. They experimentally showed that lead balls coated with a layer of silicon rubber can be used to achieve effective negative elastic modulus. Then a similar structure was proved to exhibit double-negative acoustic properties.[8] However, the resonant behaviour of these materials, which are characterized by a short bandwidth and high losses, encouraged investigating a new class of transmission-line (TL) based acoustic metamaterials. Following the work of Fang *et al*.,[9] a new unit-cell was proposed consisting of a tube with a side hole, achieving negative bulk modulus over a large bandwidth.[10] Side holes along with clamped membranes which exhibit negative dynamic mass[11,12] provided necessary and sufficient means of obtaining composite acoustic media with simultaneously negative mass density and bulk modulus.[13] Then, TL modelling was proposed to design acoustic metamaterials with no band gap, and leaky-wave antenna (LWA) applications were first envisaged.[14] Later, the theory of acoustic LWA was experimentally validated[15] and new applications were reported, such as direction finding[16] and acoustic dispersive prism.[17]

Recently, Xie *et al*. have brought the idea of single sensor sound localisation into the limelight by introducing single-sensor cocktail party listener using acoustic metamaterials, capable of separating broadband signals produced by three separate sources.[18] In the present article, we propose an alternative technique using leaky-wave antennas based on an acoustic TL metamaterial to locate the direction of sound sources with one single microphone.

The leaky-wave appellation refers to the principle of power leakage along a waveguide and it has been first developed in the 1940s (Ref. 19) in the electromagnetic realm. Owing to the high directivity and frequency scanning capability of such an antenna, it became very attractive in electromagnetics. However, LWAs based on conventional right-hand materials exhibit only positive wavenumbers and, as a consequence, have the drawback of scanning only the half-space from broadside to endfire (0, 90°). With the introduction of composite right/left-hand (CRLH) TL-metamaterials, which support both positive and negative wavenumbers, the

[a)]Electronic mail: herve.lissek@epfl.ch

backfire to endfire (–90°, 90°) electromagnetic antenna has been made possible by design.[20]

In this article the acoustic counterpart of electromagnetic LWA, exhibiting backfire to endfire radiation/reception, is exploited for direction finding. The structure of this article is as follows: first, the acoustic LWA theory and mechanism are presented and mathematically formulated to get the desired radiation efficiency and directivity. Then, a new concept of single microphone source localisation is introduced, with theoretical and numerical simulations highlighting the phenomenon. Finally, a frequency-dependent directionality is derived from experimental assessments, followed by a discussion on the practical use of such a structure.

II. ACOUSTIC LEAKY-WAVE ANTENNA

A. General description and properties

An acoustic LWA is a waveguiding structure that favours the sound power leakage through radiating openings as it propagates along its axis. Leaky-waves are usually employed in antenna applications, since the leakage phenomenon is generally associated with high directivity and therefore, their size is not constrained by the operating wavelength, but rather by the directivity specifications.[21] A simple leaky-wave structure is schematically represented in Fig. 1.

In the transmission mode (for which a source is emitting sound inside the waveguide), the sound pressure field leaking out of the waveguide, in free-field conditions, follows the form[20]

$$p(y,z) = p_0 e^{-\gamma y} e^{-jk_z z}, \tag{1}$$

where $\gamma = \alpha + j\beta$ is the complex propagation constant of the wave along the y direction, and k_z is the propagation constant perpendicular to this direction, related to β by (Fig. 1)

$$k_z \simeq \sqrt{k_0^2 - \beta^2}, \tag{2}$$

where $k_0 = \omega/c$ is the wavenumber, c being the sound velocity in the host medium, and ω the angular frequency of the wave. Equation (2) yields the following observations: if

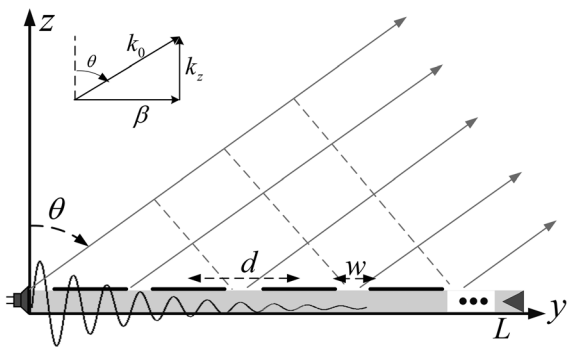

FIG. 1. Schematic representation of a leaky-wave structure. A 1D waveguide of length L along the y axis with openings of width w and a spatial spacing d. The solid and dashed lines above the structure represent the sound rays and wavefronts, respectively.

$\beta > k_0$ (the propagating wave inside the waveguide is slower than the sound velocity $v_p < c$), then k_z is imaginary and no sound is radiated outside the structure. Conversely, if $\beta < k_0$ ($v_p > c$, fast-wave), k_z is real and the wave leaks out. Thus, a slow-wave, characterized by $\beta > k_0$, is a guided wave, whereas a fast-wave, characterized by $\beta < k_0$, is a leaky-wave. The region of the dispersion diagram where the condition $\beta < k_0$ is satisfied is called the radiation region, and any waveguiding structure presenting a dispersion curve $\omega(\beta)$ inside the radiation region is considered a leaky-wave structure. Using Eq. (2), the propagation constant β is linked to the angle θ_0 of the main lobe by

$$\theta_0 \simeq \sin^{-1}(\beta/k_0). \tag{3}$$

For a dispersive medium, the quantity β/k_0 depends on frequency and therefore the main beam angle can vary as a function of frequency, this property is called frequency scanning.

B. Radiation pattern

For a 1D leaky-wave with continuous leakage along the structure (Fig. 1 with $w = d$), the radiated sound pressure towards the upper half space reads[22]

$$p_{rad}(r,\theta) = \int_0^L p_0 e^{-\gamma y} \frac{e^{-jk_0 r}}{2\pi r} dy, \tag{4}$$

where r is the distance between the observation point and a position y along the LWA. In the far field, distance r can be approximated by $r \simeq r_0 - y\sin\theta$ (in the phase term $e^{-jk_0 r}$), and by $r \simeq r_0$ for the geometric attenuation $1/2\pi r$, where r_0 is the distance between the origin $(y, z = 0)$ and the observation point. After Eq. (4), the radiated sound pressure reads

$$p_{rad}(r_0,\theta) = \frac{p_0}{\pi r_0} e^{-jk_0 r_0} e^{(-\gamma + jk_0 \sin\theta)(L/2)} \times \frac{\sinh\left[(-\gamma + jk_0\sin\theta)\frac{L}{2}\right]}{-\gamma + jk_0\sin\theta}. \tag{5}$$

Using Eq. (5) the acoustic power radiated by an infinitely long leaky-wave structure ($L \to \infty$) is proportional to

$$|p_{rad}(r_0,\theta)|^2 = \left(\frac{p_0}{2\pi r_0}\right)^2 \frac{1}{\alpha^2 + (\beta - k_0\sin\theta)^2}. \tag{6}$$

Using the radiation power pattern of Eq. (6) the half-power beamwidth $\Delta\theta$ of the structure can be derived from

$$\sin\frac{\Delta\theta}{2} = \frac{\alpha}{k_0\cos\theta_0}. \tag{7}$$

Let us now consider a periodic arrangement of open holes (Fig. 1) of width w situated between nd and $nd + w$, where $n = 0, \ldots, i$ is the index of the hole and d is the distance between two consecutive holes. The pressure radiated at an observation point (r_0, θ) is given by

$$p_{rad}(r_0,\theta) = \sum_{n=0}^{N-1} \int_{nd}^{nd+w} p_0 e^{-\gamma y} \frac{e^{-jk_0 r}}{2\pi r} dy$$
$$= \frac{p_0}{\pi r_0} e^{-jk_0 r_0} e^{(-\gamma + jk_0 \sin\theta)(w/2)} \times \frac{\sinh\left[(-\gamma + jk_0 \sin\theta)\frac{w}{2}\right]}{-\gamma + jk_0 \sin\theta} \sum_{n=0}^{N-1} e^{(-\gamma + jk_0 \sin\theta)nd}, \quad (8)$$

where N is the number of radiating holes. Comparing Eqs. (5) and (8), it appears that the arrangement of periodic holes behaves as an array of small radiating apertures. Moreover, the frequency at which the magnitude of the radiated pressure field of Eq. (5) and Eq. (8) is maximum for a given angle θ verifies Eq. (3), provided the length of the antenna or the number (N) of open holes is sufficiently large.

C. Radiation efficiency

The radiation efficiency of the leaky-wave structure is another important parameter for the design. It can be calculated by considering that the sound power sent at the input of a lossless leaky-wave structure is conserved in addition to the transmitted, reflected and radiated power ($\Psi_{in} = \Psi_{ref} + \Psi_{tran} + \Psi_{rad}$). Defining the radiation power efficiency of the leaky-wave antenna as the ratio of the radiated power to the input power, for a lossless structure with no reflection ($\Psi_{ref} = 0$) the radiation efficiency is calculated as[21]

$$\eta_{rad} = 1 - e^{-2\alpha L}, \quad (9)$$

where α is the real part of the complex propagation constant ($\gamma = \alpha + j\beta$) and accounts for the leaked power due to the radiation. The leakage factor (α) can be calculated by

$$\Psi_2 = \Psi_1 e^{-2\alpha l_{12}}, \quad (10)$$

where Ψ_1 and Ψ_2 are the average power measured in two different cross sections of the leaky-wave that are separated by length l_{12}.

Using Eq. (9) and specifying a radiation efficiency of 90%, it yields

$$\frac{L}{\lambda_0} \simeq \frac{0.18}{\alpha/k_0}. \quad (11)$$

Given a leakage factor (α), which depends on the design of the leaky-wave structure, Eq. (11) defines the necessary length to obtain a 90% radiation efficiency. Thus, the structure can be designed based on the framework introduced above to achieve a prescribed radiation efficiency.

III. CONCEPT OF SINGLE-MICROPHONE DIRECTION FINDING

A. Proposed design

The proposed single-microphone direction finding concept is illustrated in Fig. 2, where a microphone is wall-mounted close to one termination, the two terminations presenting anechoic conditions, with a layer of mineral wool.

The structure is composed of an acoustic TL metamaterial with subwavelength unit-cells made of small ducts of radius $r_{waveguide}$ and length $d_{unit-cell}$, comprising a membrane (of same cross-section, and thickness $t_{membrane}$), and a transverse cylindrical open-channel connected on one side of the duct (also denoted "stubs") of radius r_{stub} and length L_{stub}. Each unit-cell can be modelled as series mass and parallel compliance (supporting the right-hand or positive index propagation), combined with series compliance and parallel mass (supporting left-hand or negative index propagation), as explained in Refs. 14 and 17. Thus, it behaves as an acoustic bandpass filter. The transverse open ducts, which are modelled by radiation impedances, make the structure behave as a leaky-wave antenna, allowing the radiation of an acoustic wave to the ambient medium. Schematically, a leakage can be modelled as an acoustic radiation resistance, in series with the acoustic mass representing the acoustic impedance of the stub.[17] For the sake of simplicity, we do not consider here mutual coupling between consecutive stubs, assuming they are distant enough. Although the radiation resistance does not affect the TL metamaterial behaviour, it physically provides the appropriate condition for power leakage along a direction of radiation that depends on the frequency of sound. Here, the leaky-wave mechanism favours a given radiation direction depending on the refractive indices assigned to each frequency of the input wave by the TL metamaterial, after Eq. (3).

This structure is similar to the one proposed in Ref. 14. Here, however, flanged cylindrical ducts are substituted for the axisymmetric open channels.[16,17] This modification has been mainly proposed to prevent the monopolar behaviour of the axisymmetric structure, which is expected to present an omnidirectional radiation pattern. Indeed, the radiation pattern of such an axisymmetric leaky-wave antenna is "doughnut-shaped," with constant directivity around the

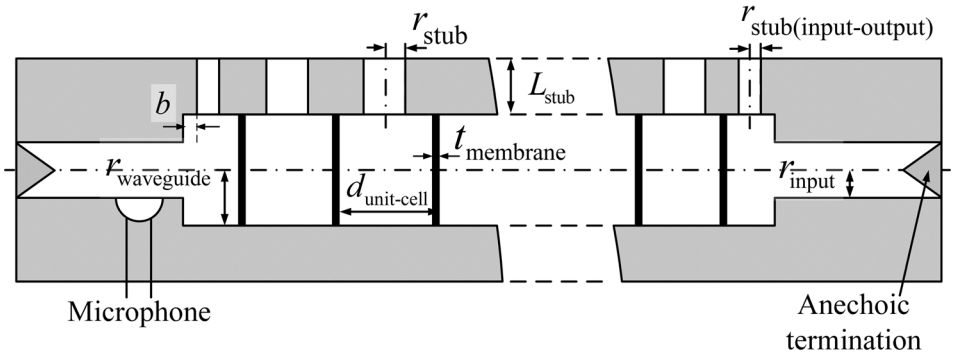

FIG. 2. 2D schematic representation of the single-microphone direction finding concept, based on the periodic structure inspired by Refs. 13 and 14. A microphone is inserted at the left termination of the waveguide, and absorbing material (mineral wool) fills the two terminations.

TABLE I. Dimensions of the designed structure.

Dimension	Symbol	Value (mm)
Unit-cell length	$d_{unit-cell}$	32.00
Duct radius	$r_{waveguide}$	9.06
Terminating ducts radius	r_{input}	5.54
Stub radius	r_{stub}	4.00
Terminating stubs radius	$r_{stub(input-output)}$	2.90
Stub length	L_{stub}	12.50
First stub position	b	1.10
Membrane thickness	$t_{membrane}$	0.125

symmetry axis of the structure. The proposed geometrical modification of the new LWA structure, with open channels facing only the positive z direction, is then intended to sense sound waves only from one half-space. Moreover, the LWA structure is flanged to on an acoustically hard surface, yielding two effects. First, the flanged hard surface suppresses the back lobes, thus preventing the structure from radiating to the back side. Second, it increases the radiated power towards the upper half-space.

B. Numerical results

1. Presentation of the numerical model

Based on the design procedure explained in Refs. 14 and 17, the structure of Fig. 2 with 10 unit-cells and an approximate length of 2λ is designed. Note that the input and output cross sections of the waveguide are designed smaller than the main duct to ensure perfect impedance matching with the leaky-wave structure. Moreover, the LWA presents a periodic structure, except for the first and last stubs. Indeed, in order to comply with the unit-cell definition, the first and the last transverse ducts should be geometrically half of the other stubs.[14] Nevertheless, in order to improve impedance matching, the first and last stubs' dimensions have been modified, leading to the final dimensions presented in Table I (the material properties are also given in Table II). The finite-element simulation (FEM) of the structure is carried out using COMSOL MULTIPHYSICS where the acoustic-shell interaction physics module in frequency domain is used for simulating the full structure. The open end of the stubs are flanged to an acoustic hard surface and the full structure, as well as the acoustic domain represented by a half-sphere are bounded by a perfectly matched layer (PML) to realize non-reflecting boundaries. An acoustic background pressure field is applied to the acoustic domain, and the sound pressure computed at a given position near the input of the leaky-wave is the output of the model. The FEM results are then compared to the analytical model presented in Sec. II, where the value of γ is processed from the TL model.[14,17]

TABLE II. Material properties of the designed structure.

Physical quantity	Symbol	Value	Unit
Mass density of air	ρ	1.188	kg/m^3
Bulk modulus of air	K	137.4	kPa
Celerity of sound in the air	c	340	m/s
Membrane Young's modulus	E	2.758	GPa
Poisson ratio	ν	0.34	—
Membrane mass density	ρ_m	1420	kg/m^3

2. Radiating mode

First used in the transmitting mode, a small sound source is substituted to the microphone of Fig. 2. The far-field radiation pattern of the structure is shown in Fig. 3 for monochromatic sound sources with three different frequencies: (a-1), (b-i) 900 Hz; (a-ii), (b-ii) 1000 Hz; and (a-iii), (b-iii) 1100 Hz, and it can be seen that the direction of radiation actually varies with frequency. Figure 3(a) gives a polar representation in the yz-plane, which compares the radiation patterns derived using FEM, theoretical model of Eq. (8) (the value of γ is retrieved using TL method)[17] and experimental data of Sec. IV. These figures confirm that all three methods qualitatively agree, although small discrepancies between FEM and analytical method can be seen. Indeed, the theoretical relation of Eq. (8) is based on 1D model, whereas the FEM considers a 3D geometry which might result in disagreement between actual distribution of pressure field inside the waveguide and in the analytical model of Eq. (1), and consequently, discrepancies in the far-field radiation pattern. Figure 3(b) represents the 3D radiation pattern of the structure. It shows that, by increasing the frequency of the sound source, the radiation pattern actually scans the upper hemisphere from backward to forward. The amplitude of the radiated sound pressure is maximal at a given angle, monotonically varying with frequency, according to Eq. (3). Using Eqs. (2) and (3) and replacing the denominator of Eq. (7) by $k_0 \cos\theta_0 = \sqrt{k_0^2 - \beta^2}$ yields the relation between half-power beamwidth (α 1/directivity) and frequency for LWA of given length:

$$\sin\frac{\Delta\theta}{2} = \frac{\alpha}{\sqrt{k_0^2 - \beta^2}}. \tag{12}$$

For a structure with constant Leaky factor (α), the directivity depends on $\sqrt{k_0^2 - \beta^2}$ behaviour which tends to zero when $k_0^2 \approx \beta^2$ (the boundaries of the leaky region) and becomes maximum when $\beta \approx 0$ (see Ref. 17). Then, starting from backward the directivity first increases with frequency, having the maximum directivity near broadside, and decreases in the forward direction. Moreover, substituting Eq. (11) in Eq. (7), the directivity of the acoustic leaky-wave antenna can be derived as a function of length L,

$$\sin\frac{\Delta\theta}{2} = \frac{0.18\lambda_0}{L\cos\theta_0}. \tag{13}$$

Here, the directivity increases by increasing the length of the leaky-wave structure

3. Receiving mode

Let us now consider the leaky-wave structure when used in the receiving mode, as presented in Fig. 2. A plane wave sound field with varying directions θ in the yz plane is considered as the input of the model, and the sound power

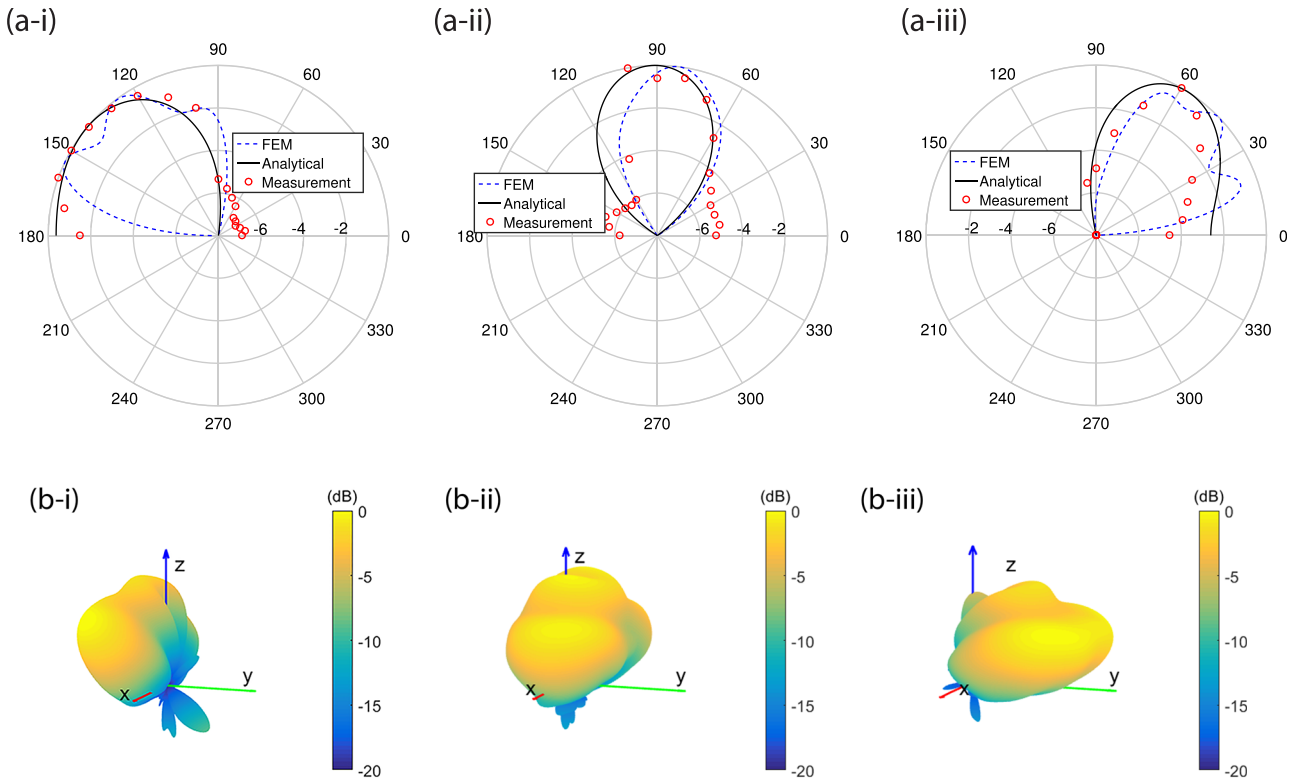

FIG. 3. (Color online) (a) The polar representation of the far-field radiation pattern of the structure in the yz-plane for three distinct frequencies: (a-i) 900 Hz, (a-ii) 1000 Hz, and (a-iii) 1100 Hz. Each radiation pattern has been normalized to its maximum and then levelled to 8 dB. (b) Maximum-normalized 3D far-field radiation patterns of the structure, extracted from COMSOL simulations, provide information about the directivity of the structure as an acoustic antenna: (b-i) 900 Hz, (b-ii) 1000 Hz, and (b-iii) 1100 Hz.

spectrum sensed at the microphone position is the output of the model for each angular direction θ. The normalized sound power spectra are derived from the FEM output data and illustrated in Fig. 4(a) for three different angles of incidence. These results are also compared to the ones processed with the theoretical model of Eq. (8). Based on reciprocity Eq. (8) holds for both transmitting and receiving modes with $w = 2r_{stub}$, $d = d_{unit-cell}$, and the value of γ retrieved using the TL method.[17] As discussed before, the small discrepancies can be justified by the differences between the 1D configuration used in the analytical formulations and the actual 3D configuration of the FEM. Moreover, the value of γ retrieved with the TL modeling might also result in small inaccuracies, which may be another source of errors. It can be seen that, for each incident angle, the power spectra sensed at the microphone position presents a lobe with maximal amplitude at a given frequency and this frequency varies with the angle θ according to Eq. (3). Based on the received power spectra of the LWA, the curves of Fig. 4(b) are derived and depict the dependence of frequency of the maximum amplitude of received power [denoted $max(PWR)$ in the following] with respect to incident angle for FEM and theoretical data. This confirms the functionality of the LWA as a single microphone sound source localizer.

It is noticeable that the received power spectra present, at angular directions near broadside, a double-bump [see the curve corresponding to the 0° direction in Fig. 4(a)]. This phenomenon is due to the occurrence of a bandgap which is the consequence of unbalanced series and parallel resonances in

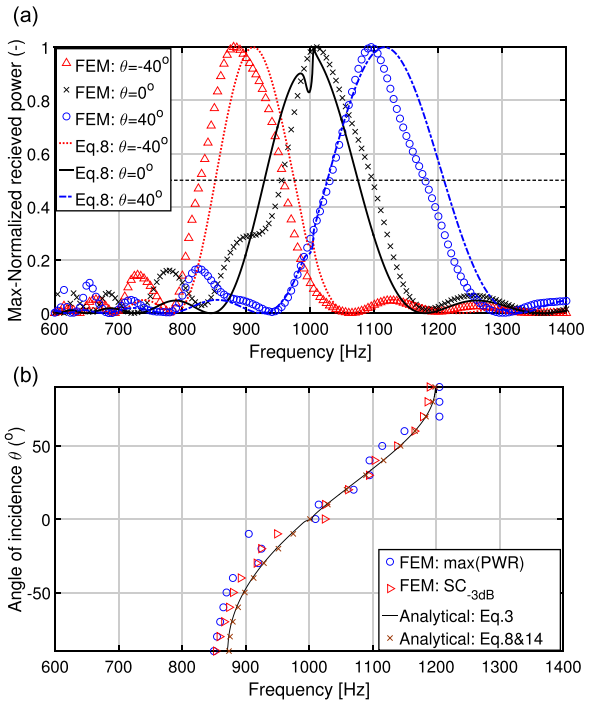

FIG. 4. (Color online) (a) Received power spectra sensed by the microphone in the LWA for the different plane wave incident angles (θ). Results of FEM are compared to Eq. (8). (b) Frequency-direction curve is presented, every 10°, for FEM and analytical method. Two different strategies are used to derive these data: frequency of the maximum received power amplitude [$max(PWR)$] versus incident angle and SC_{-3dB} of the received power versus incident angle.

the TL metamaterial design. Indeed, the geometrical dimensions and material properties have been chosen so as to be feasible in practice with readily available materials, which makes the unbalanced condition unavoidable. To overcome the potential ambiguity in the direction estimation, resulting from the secondary lobes observed on the power spectra, a new method for processing the power spectra is proposed. As the antenna behaves as a selective bandpass filter, the spectral centroid ($SC_{-3\,\mathrm{dB}}$) of the received power can be substituted for the estimation of the frequency at which the maximum power is received. For each angular position, the frequency boundaries ($f_{-3\,\mathrm{dB},min}$, $f_{-3\,\mathrm{dB},max}$) are first determined as the frequencies for which half of the maximum power is received at the sensing position. Then the 3 dB spectral centroid is computed as

$$SC_{-3\,\mathrm{dB}} = \frac{\sum_{f=f_{-3\,\mathrm{dB},min}}^{f_{-3\,\mathrm{dB},max}} fP(f)}{\sum_{f=f_{-3\,\mathrm{dB},min}}^{f_{-3\,\mathrm{dB},max}} P(f)}. \quad (14)$$

This technique may be very useful in presence of noisy experimental data as in Sec. IV. Therefore, we propose to validate this method by comparing the direction vs frequency functions obtained with the FEM and analytical models as illustrated in Fig. 4(b).

The presented numerical and analytical results confirm that the designed structure is capable of steering towards the direction of the incoming sound signal using only a single microphone. This interesting method may challenge existing techniques relying on multiple sensors beamforming for sound source localisation. It may also be compared to interference-type (shotgun) microphones, which use interferences throughout a conventional cylindrical waveguide to increase the directivity of the sensor.[23] In Sec. IV, this result will serve as a reference and compared with the frequency-direction mapping achieved with an experimental prototype.

IV. EXPERIMENTAL VALIDATION

A. Experimental prototype

An experimental prototype following the design presented in Fig. 2 is fabricated by stacking 10 unit-cells made of aluminum, as illustrated on Fig. 5(a). To assemble the full structure, each membrane (DuPont Kapton FPC) is glued on a 3D printed support, and squeezed between two adjacent unit-cells using four screws as in Fig. 5(b). The 3D printed support in Fig. 5(c) is designed to decouple the stress applied on the membrane by the adjacent unit-cells. Instead, uniform gluing of the membrane over the support ensures uniform stress over the circumference of each membrane, and almost uniform clamping condition can be achieved for all membranes. This method is more practical and straightforward compared to the one relying on individual alignment of resonant frequency of each membrane proposed in Ref. 17. To complete the assembly of the prototype, the two extremities of the fabricated structure are filled with layers of mineral wool to simulate anechoic boundary conditions, and a PCB Piezotronics 130D20 ICP

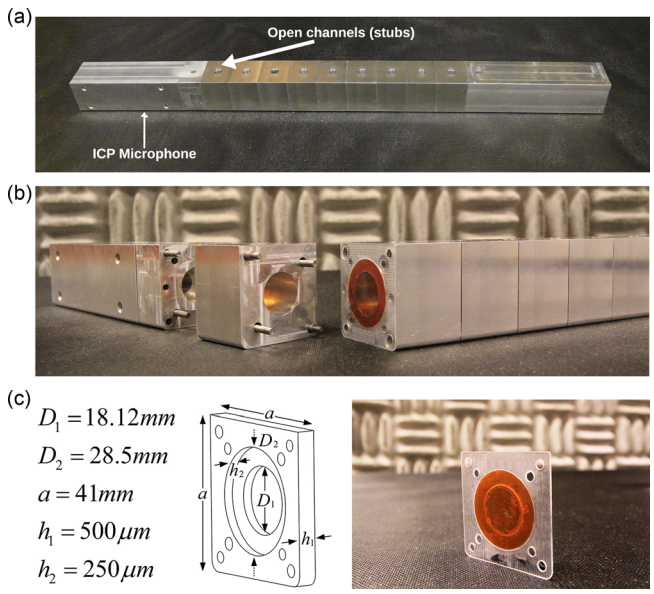

FIG. 5. (Color online) (a) Picture of the fabricated prototype: the holes on the top side correspond to the open channels (stubs), the ICP microphone used as the LWA single sensor being flush-mounted at one termination, on the opposite side (not visible here). (b) Picture of a disassembled LWA prototype, presenting a membrane glued to a support which is sandwiched between two unit-cells. (c) Picture of the membrane support as well as its schematic representation and geometrical dimensions.

microphone is flush-mounted at one termination of the structure, and used as the single sensor of the LWA. Finally, it is flanged to a wooden panel of dimensions 50 cm × 50 cm, which mimics the hard boundary conditions considered in the FEM model, while suppressing the back lobes.

B. Experimental setup

To measure the performance of the fabricated prototype as a single-microphone direction finding, the LWA mounted on a panel is installed on a turntable (Bruel & Kjaer type 5960, remote-controlled through a controller type 5949) in an anechoic chamber, and a loudspeaker (sound source) is installed at 4 m from the center of the leaky-wave, as illustrated in Fig. 6. The sound generation and the microphone signal acquisition are operated with a Bruel & Kjaer type 3160 Pulse multichannel analyzer. The FFT analysis is set on 3200 points within the [600–1400 Hz] frequency range, thus a frequency resolution of 0.25 Hz, and the signal generator delivers a sweep sine signal within the frequency range [600–1400 Hz] to the loudspeaker.

C. Measurement results

For each angular position of the turntable, the power spectrum $P(f)$ of the received signal is processed. Figure 7(a) presents the normalized power spectra measured for different orientations of the turntable. As explained in Sec. III B, the main lobe observed on the power spectrum measurement presents a frequency, that can then be mapped to the orientation of the turntable. It is noticeable that, for each orientation, the antenna presents a relatively narrow beam width, except around 0° where two lobes are visible. This can be explained by a misalignment of the elements of the LWA

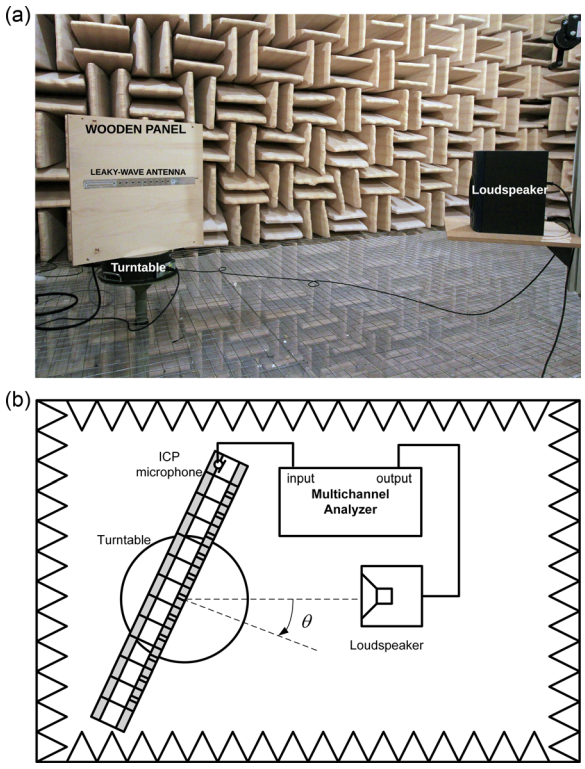

FIG. 6. (Color online) (a) Measurement setup in the anechoic chamber: the leaky-wave antenna is wall-mounted to a wooden panel, suppressing the back lobe and acting as a support, the whole being fixed on a turntable in front of a loudspeaker used as a sound source. (b) Schematic description of the experimental setup.

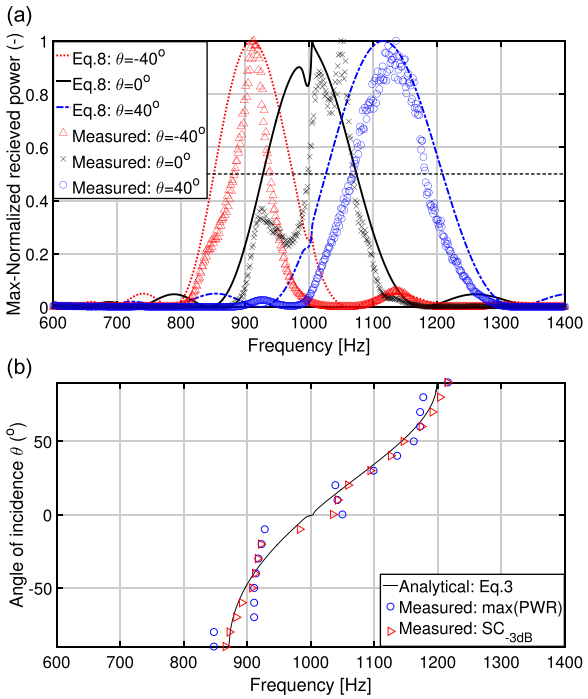

FIG. 7. (Color online) (a) Measured power spectra sensed by the microphone in the LWA for different angular positions of the turntable θ. (The experimental data are shown every five samples). Experimental results are compared to theoretical values of Eq. (8). (b) Frequency-direction curve of measured data is presented every 10° derived by two different methods: frequency of the maximum received power amplitude versus incident angle and received power SC_{-3dB} versus incident angle. The analytical expected curve is also presented for comparison.

(membranes and stubs), resulting in the occurrence of a band-gap around the transition frequency and emergence of second lobe in the received power spectra.

D. Frequency-source direction mapping

With a view to assessing the single-microphone direction finding functionality of the LWA, the spectral centroid and $max(PWR)$ are derived from the power amplitude received by the ICP microphone for each orientation θ of the turntable, and compared to the theoretical value obtained from Eq. (3). Figure 7(b) presents the frequency-direction curve of the LWA which confirms the good agreement between theoretical and measured data. Moreover, in order to overcome the ambiguity resulting from the emergence of a second lobe near the broadside direction, the $SC_{-3\,\mathrm{dB}}$ is derived from experimental data using Eq. (14) and is plotted against the angular position of the turntable. As expected, the $SC_{-3\,\mathrm{dB}}$ derived from the measured data shows smoother variations compared to the $max(PWR)$, and is in closer agreement with the theoretical curve.

E. Discussion

The results of Figs. 4(b) and 7(b) show that the theoretical, FEM and experimental data, present monotonically-increasing directions θ as a function of frequency f, which can then be used for single-microphone direction finding applications. Furthermore, the frequency-direction mapping obtained with experimental and simulation data follows the theoretical trend, which also validates the theoretical formulas. The small discrepancies observed between measured data and the theoretical trend can be explained by two reasons: the first reason might be the differences in the fabricated prototype compared to the optimal design parameters considered in the theoretical formulation, especially the difficulty to ensure perfectly uniform clamped boundary conditions on the membranes in the experimental prototype. The second reason might be the differences between the simulation and experimental conditions. Indeed, the imperfect anechoic conditions in the waveguide extremities, as well as the likely imperfect frequency response of the loudspeaker may significantly differ from the simulation condition. Due to the listed problems and occurrence of second lobe near the broadside [particularly visible in the measured results in Fig. 7(a)], a statistical method of spectral centroid of the data is used to get smoother frequency-direction curves.

V. CONCLUSION

This study introduces a single-microphone direction finder as an interesting novel application of acoustic TL metamaterials. It consists in a periodic structure composed of vibrating membranes along a waveguide, and side open channels allowing sound leakage along the structure. In the receiving mode, it is shown that such device can be used as a single-microphone direction finder, without resorting to multiple-sensors beam-steering techniques. The concept is validated with an experimental prototype, the sound pressure

sensed by the single microphone showing an angle-dependent power spectrum, highlighting a monotonically increasing relationship between the angle of observation and the frequency. The frequency-direction mapping, also derived using spectral centroid ($SC_{-3\,\mathrm{dB}}$) of the received power, shows a smoother monotonic behaviour. It should also be emphasized that those results have been confirmed with several measurements, after mounting/dismantling of the prototypes, highlighting simplicity of the implementation and robustness of the LWA structure. Such device can be seen as an interesting alternative to the state-of-the-art techniques for sound source localization, and may find direct applications to sonar. Moreover, since acoustic and electromagnetic leaky-wave antenna are based on similar physics, they share the same waveguiding structure as a host medium. This suggests that a conventional (RH) electromagnetic leaky-wave radiating in the forward direction can turn into an acoustic leaky-wave antenna. However, achieving electromagnetic/acoustic leaky-wave antenna with both RH/LH behaviour radiating from backward to forward is a remaining challenge. This article may encourage future development with a view to merge acoustic/electromagnetic RH/LH leaky-wave antennas within the same structure, and proposing a new generation of mixed radar-sonar concepts based on leaky-wave concept.

ACKNOWLEDGMENTS

This work was supported by the Swiss National Science Foundation (SNSF), under Grant Agreement No. 200020-138086. The authors would like to thank Jean-Paul Brugger, Roland Dupuis, and Karim Collomb of the AEM workshop for their help in the construction of the prototype, and also Patrick Roe for his help in proofreading the paper.

[1]S. Zhang, C. Xia, and N. Fang, "Broadband acoustic cloak for ultrasound waves," Phys. Rev. Lett. **106**(2), 024301 (2011).
[2]J. Li, L. Fok, X. Yin, G. Bartal, and X. Zhang, "Experimental demonstration of an acoustic magnifying hyperlens," Nat. Mater. **8**(12), 931–934 (2009).
[3]J. Mei, G. Ma, M. Yang, Z. Yang, W. Wen, and P. Sheng, "Dark acoustic metamaterials as super absorbers for low-frequency sound," Nat. Commun. **3**, 756 (2012).
[4]Y. Li, B. Liang, Z. M. Gu, X. Y. Zou, and J. C. Cheng, "Reflected wavefront manipulation based on ultrathin planar acoustic metasurfaces," Sci. Rep. **3**, 2546 (2013).
[5]B. I. Popa and S. A. Cummer, "A Non-reciprocal and highly nonlinear active acoustic metamaterials," Nat. Commun. **5**, 3398 (2014).
[6]R. Fleury, D. L. Sounas, C. F. Sieck, M. R. Haberman, and A. Alù, "Sound isolation and giant linear nonreciprocity in a compact acoustic circulator," Science **343**(6170), 516–519 (2014).
[7]Z. Liu, X. Zhang, Y. Mao, Y. Y. Zhu, Z. Yang, C. T. Chan, and P. Sheng, "Locally resonant sonic materials," Science **289**(5485), 1734–1736 (2000).
[8]J. Li and C. T. Chan, "Double-negative acoustic metamaterial," Phys. Rev. E **70**(5), 055602 (2004).
[9]N. Fang, D. Xi, J. Xu, M. Ambati, W. Srituravanich, C. Sun, and X. Zhang, "Ultrasonic metamaterials with negative modulus," Nat. Mater. **5**(6), 452–456 (2006).
[10]S. H. Lee, C. M. Park, Y. M. Seo, Z. G. Wang, and C. K. Kim, "Acoustic metamaterial with negative modulus," J. Phys.: Condens. Matter **21**(17), 175704 (2009).
[11]Z. Yang, J. Mei, M. Yang, N. H. Chan, and P. Sheng, "Membrane-type acoustic metamaterial with negative dynamic mass," Phys. Rev. Lett. **101**(20), 204301 (2008).
[12]S. H. Lee, C. M. Park, Y. M. Seo, Z. G. Wang, and C. K. Kim, "Acoustic metamaterial with negative density," Phys. Lett. A **373**(48), 4464–4469 (2009).
[13]S. H. Lee, C. M. Park, Y. M. Seo, Z. G. Wang, and C. K. Kim, "Composite acoustic medium with simultaneously negative density and modulus," Phys. Rev. Lett. **104**(5), 054301 (2010).
[14]F. Bongard, H. Lissek, and J. R. Mosig, "Acoustic transmission line metamaterial with negative/zero/positive refractive index," Phys. Rev. B **82**(9), 094306 (2010).
[15]C. J. Naify, C. N. Layman, T. P. Martin, M. Nicholas, D. C. Calvo, and G. J. Orris, "Experimental realization of a variable index transmission line metamaterial as an acoustic leaky-wave antenna," Appl. Phys. Lett. **102**(20), 203508 (2013).
[16]H. Esfahlani, S. Karkar, and H. Lissek, "Acoustic leaky-wave antenna," in *Proceedings of IEEE 8th International Congress on Advanced Electromagnetic Materials in Microwaves and Optics (METAMATERIALS)* (2014), pp. 403–405.
[17]H. Esfahlani, S. Karkar, H. Lissek, and J. R. Mosig, "Acoustic dispersive prism," Sci. Rep. **6**, 18911 (2016).
[18]Y. Xie, T. H. Tsai, A. Konneker, B. I. Popa, D. J. Brady, and S. A. Cummer, "Single-sensor multispeaker listening with acoustic metamaterials," Proc. Natl. Acad. Sci. **112**(34), 10595–10598 (2015).
[19]W. W. Hansen, "Radiating electromagnetic wave guide," U.S. patent No. 2,402,622 (1946).
[20]C. Caloz and T. Itoh, *Electromagnetic Metamaterials: Transmission Line Theory and Microwave Applications* (Wiley, Hoboken, NJ, 2005), Chap. 6, pp. 261–275.
[21]A. A. Oliner, D. R. Jackson, and J. L. Volakis, *Antenna Engineering Handbook*, 4th ed. (McGraw Hill, New York, 2007), Chap. 11, p. 286.
[22]P. M. Morse and K. U. Ingard, *Theoretical Acoustics* (Princeton University Press, Princeton, 1968), Chap. 7, pp. 319–322.
[23]J. Eargle, *The Microphone Book* (Focal Press, Oxford, UK, 2005), Chap. 6, pp. 91–96.